

Microcosmic mechanism of reinforced interfacial transition zone in SFP materials An insight from micro- and nano-scale tests

Liu, Xiaoyu; Wu, Kuanghuai; Ni, Botao; Li, Yi; Yue, Yunpeng; Cai, Xu; Ren, Fengming

10.1016/j.conbuildmat.2025.141521

Publication date

Document Version Final published version

Published in Construction and Building Materials

Citation (APA)
Liu, X., Wu, K., Ni, B., Li, Y., Yue, Y., Cai, X., & Ren, F. (2025). Microcosmic mechanism of reinforced interfacial transition zone in SFP materials: An insight from micro- and nano-scale tests. *Construction and* Building Materials, 481, Article 141521. https://doi.org/10.1016/j.conbuildmat.2025.141521

Important note

To cite this publication, please use the final published version (if applicable). Please check the document version above.

Other than for strictly personal use, it is not permitted to download, forward or distribute the text or part of it, without the consent of the author(s) and/or copyright holder(s), unless the work is under an open content license such as Creative Commons.

Takedown policy

Please contact us and provide details if you believe this document breaches copyrights. We will remove access to the work immediately and investigate your claim.

Green Open Access added to TU Delft Institutional Repository 'You share, we take care!' - Taverne project

https://www.openaccess.nl/en/you-share-we-take-care

Otherwise as indicated in the copyright section: the publisher is the copyright holder of this work and the author uses the Dutch legislation to make this work public.

\$ SUPER

Contents lists available at ScienceDirect

Construction and Building Materials

journal homepage: www.elsevier.com/locate/conbuildmat





Microcosmic mechanism of reinforced interfacial transition zone in SFP materials: An insight from micro- and nano-scale tests

Xiaoyu Liu^a, Kuanghuai Wu^{a,*}, Botao Ni^b, Yi Li^c, Yunpeng Yue^a, Xu Cai^a, Fengming Ren^{a,*}

- ^a School of Civil Engineering and Transportation, Guangzhou University, Guangzhou 510006, China
- ^b Yong Fu Construction Engineering Group Co., Ltd., Fuzhou 350000, China
- ^c Section of Pavement Engineering, Faculty of Civil Engineering & Geosciences, Delft University of Technology, Stevinweg 1, Delft 2628 CN, the Netherlands

ARTICLE INFO

Keywords: Semi-flexible pavement Interface transition zone Asphalt-grout interface Aggregate-asphalt interface Interface enhancement

ABSTRACT

Semi-flexible pavement (SFP) is extensively used in airport and tunnel pavements due to its high strength and toughness. As a multiphase composite material, SFP contains widely distributed aggregate-asphalt interface transition zones (ITZ) and asphalt-grout ITZ. These ITZs are the weakest areas in SFP and are susceptible to cracking during operation. To enhance the crack resistance of SFP, this paper proposes an interface immersion method to immerse the porous asphalt mixtures in a silane coupling agent before grouting. However, the cracking mechanism and interface enhancement process of the ITZ in SFP are not clear. This paper employs atomic force microscopy (AFM), scanning electron microscopy (SEM), energy dispersive X-ray spectroscopy (EDS), and nanoindentation (NI) to analyze the micro- and nanoscale properties of the aggregate-asphalt ITZ and asphalt-grout ITZ before and after interface reinforcement. Experiment results show that the aggregate-asphalt ITZ exhibits minimal interaction before and after enhancement, with the primary interaction occurring in the asphalt-grout ITZ, which has superior adhesion. Grout diffusion is more pronounced in the asphalt-grout ITZ, where cracks are significantly reduced after reinforcement. The element distribution in the aggregate-asphalt ITZ is uniform with a gradual transition, while the asphalt-grout ITZ shows a denser, more continuous distribution after surface immersion, enhancing mechanical properties. The width of the aggregate-asphalt ITZ remains constant (60-90 µm), while the asphalt-grout ITZ width increases notably after modification (from 60 to 90 µm to 90-120 μm). The research results can provide theoretical support for SFP design and maintenance.

1. Introduction

Semi-flexible pavement (SFP) is a seamless wearing course made from porous asphalt mixtures (PAM), typically containing 20–30 % air voids, impregnated with a specialized cement-based grout material [1–3]. This structure offers enhanced rutting resistance compared to traditional dense-graded asphalt mixtures [4,5]. Additionally, it exhibits strong load-bearing capabilities, making it well-suited for high-traffic applications [6–8]. With increasing traffic volumes and loads, SFP is increasingly considered for high-stress areas such as heavy-load pavements, intersections, bus stops, and other specialized sections [9,10].

A significant challenge in SFP is the vulnerability of the interface transition zone (ITZ) [11–13], which is prone to cracking under mechanical stresses [14]. Zhang et al. [15] investigated the crack resistance

of asphalt mortar and the asphalt-aggregate interface using SFP materials. The results showed that an increase in the fracture energy of both asphalt mortar and the asphalt-aggregate interface effectively delayed the crack propagation rate. Zhang et al. [16] simulated the freeze-thaw damage process of SFP in real-use scenarios and used CT scanning to observe structural changes during freeze-thaw cycles. The results show that the reduction of cement-asphalt interface adhesion and the frost heave of JGM301 were identified as key factors contributing to SFP damage during freeze-thaw cycles. SFP is a multi-phase composite, involving two critical ITZs: the aggregate-asphalt ITZ and the asphalt-grout ITZ [15,17]. These interface regions are crucial for the overall performance of SFP. However, specific weaknesses within the ITZs, and which ITZ is more susceptible to cracking are not clear, complicating the prediction and mitigation of failure mechanisms in SFP

E-mail addresses: xiaoyuliu@gzhu.edu.cn (X. Liu), wukuanghuai@163.com (K. Wu), 226939462@qq.com (B. Ni), Y.Li-41@tudelft.nl (Y. Li), yueyunpeng@gzhu.edu.cn (Y. Yue), cx_caixu@163.com (X. Cai), rfm@gzhu.edu.cn (F. Ren).

^{*} Corresponding authors.

Г181.

Enhancing the ITZ through interface modification has been shown to improve the overall performance of SFP [19-21]. Yang et al. [22] developed an interfacial modifier mixed into grout to mold SFP and found that the shear performance of SFP was significantly improved. Previous research has shown that silane coupling agents can significantly improve the strength of cementitious materials, and then improving the strength of cementitious grouts can also significantly improve the mechanical properties of SFP [23]. To examine the bonding properties between porous asphalt mixture (PAM) and grout materials in SFP, Liu et al. [24] evaluated the mechanical properties of SFP using three types of grout materials, considering PAM treated with a silane coupling agent solution. The results show that the interfacial bonding strength between asphalt and grout significantly influences SFP's mechanical properties. Follow-up research in [25] investigated SFP's cracking resistance through dynamic modulus and four-point bending fatigue tests after interface modification, revealing that the proposed method significantly enhances crack resistance in SFP with low-strength grout materials. However, the mechanisms of interface modification at microscopic and nanoscopic scales remain unclear.

Advanced techniques such as atomic force microscopy (AFM) [26], scanning electron microscopy (SEM) [27,28], energy-dispersive X-ray spectroscopy (EDS) [29], and nanoindentation (NI) [30-32] have been employed to examine interface properties at these scales. Lv et al. [33] used AFM to analyze the surface morphology of asphalt at different aging times, revealing that the bee structure effectively explains the microstructural characteristics and aging evolution. Huang et al. [34] investigated the ITZs in recycled concrete aggregate asphalt mixtures using NI tests and found that aggregate composition and morphology affect the ITZ and adhesion between recycled concrete aggregate and asphalt. However, the interface properties and chemical composition of the aggregate-asphalt and asphalt-grout ITZs in SFP material remain to be characterized. Therefore, investigating the micro- and nanoscopic characteristics and modification mechanisms of both the aggregate-asphalt and asphalt-grout ITZs in SFP is essential to develop more effective interface enhancement strategies.

This paper investigates the microstructural characteristics of the composite interface in SFP at the micro- and nano-scale. To enhance the mechanical properties of the ITZ, an immersion method is proposed for interfacial modification. The aggregate-asphalt and asphalt-grout ITZs in SFP materials are analyzed through various tests before and after interface enhancement. In addition, the chemical mechanisms and molecular interactions of the interfacial modification are discussed in this study, focusing on the interactions between the silane coupling agent and the composite interface. By linking these microstructural insights to

macroscopic performance, this research seeks to provide strategies for improving the durability and resilience of SFP in road construction. Fig. 1 illustrates the flowchart of the laboratory experimental procedure. The structure of this study is as follows: Section 2 provides an overview of the micro- and nano-mechanics tests on SFP materials using AFM for adhesion performance, SEM for microscopic morphology, EDS for chemical composition, and NI for interface characterization, along with the introduction of the proposed interfacial immersion method. Section 4 presents the results of the micro- and nano-scale tests on the aggregate-asphalt and asphalt-grout ITZs in SFP with interfacial modifiers and discusses the interfacial modification mechanism in the ITZs after applying the interface modifiers. Section 5 concludes the study.

2. Materials

2.1. Asphalt and aggregate

A representative SBS-modified asphalt sample was selected for this study, with its parameters detailed in Table 1. The coarse aggregates used were natural diabase. The particle size distribution of the PAM specimens is as follows: aggregates within the 9.5–13.6 mm range account for 63.1 %, while those in the 4.75–9.5 mm and 2.36–4.75 mm ranges constitute 24.9 % and 8.5 %, respectively. The mineral powder makes up 3.5 % of the mixture, with a bitumen-to-aggregate ratio of 3.6 %. The void ratio of the PAM specimens, measured according to the Chinese standard JT/T E20–2017 [35], ranges from 28 % to 30 %.

2.2. Grout materials

Table 2 presents the specifications for the grout material, the compressive, flexural, and tensile strengths of the grout materials were evaluated in accordance with the Chinese standard JTG 3420–2020

Table 1Specifications of the SBS-modified asphalt.

Properties	Experiment results
Penetration @25°C,100 g, and 5 s (0.1 mm)	54.4
Penetration index	0.06
Ductility @5°C and 5 cm/min (cm)	32.0
Elastic recovery ratio @25°C (%)	95.0
Segregation (softening point) @163°C and 48 h (°C)	1
Softening point R&B (°C)	88.5
Viscosity @135°C (pa.s)	2.36

Note: The asphalt was produced by Shell Xinyue (Foshan) Asphalt Co., Ltd.

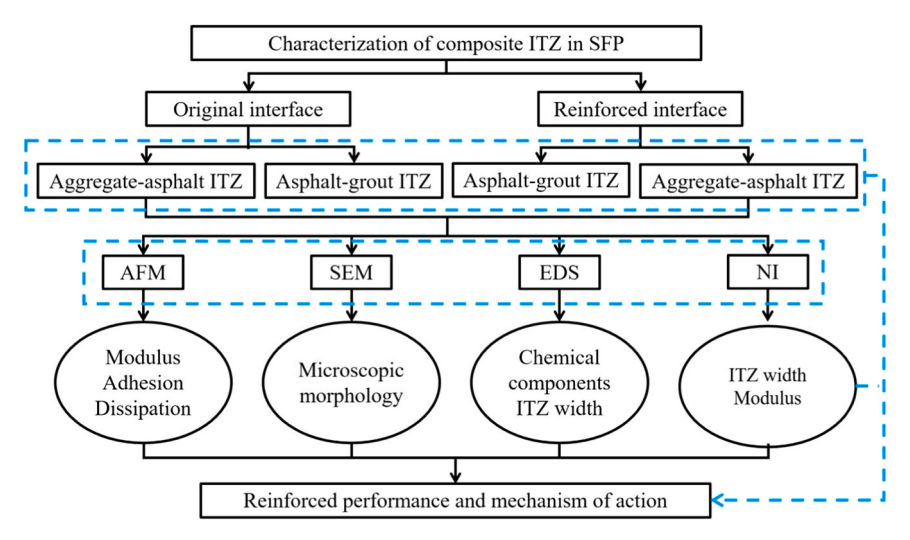


Fig. 1. Flowchart of the laboratory experimental procedure.

Table 2 Specifications of the grout material.

Materials	water-binder ratio	Tensile strength (MPa)	Compressive strength (28 d) (MPa)	Fluidity (s)	Flexural strength (28 d) (MPa)
Grout materials	0.32	1.11	36.88	10	8.30

Note: The grout material was produced by Sobute New Materials Co., Ltd.

[36]. The cement-based grout was mixed using a laboratory-scale cement mortar mixer and then poured into the PAM specimens.

2.3. Interfacial immersion method

Our prior studies [24] demonstrated that treating PAM specimens with a silane coupling agent solution before grouting enhances the mechanical characteristics of the composite interface in SFP materials. In this study, the KH-570 silane coupling agent was used to improve the asphalt-grout interface. The silane coupling agent solution was prepared by mixing 72 % methanol, 20 % silane coupling agent, and 8 % water to ensure optimal hydrolysis. The PAM samples were immersed in this solution for one hour. After immersion, the PAM was grouted to form the SFP specimens. Table 3 lists the types of laboratory experiment cases for micro and nano testing.

3. Methods

3.1. Sample preparation

3.1.1. AFM and NI samples

The SFP specimens were cored and cut into 1 cm high cubes to prepare the AFM and NI specimens. Vertical variations in the micro- and nano-mechanical properties of the SFP, both before and after interface modification, were captured using AFM and NI. This approach enabled the characterization of microstructural features and modulus changes across different ITZs within the SFP. A final SFP specimen is shown in Fig. 3.

3.1.2. SEM-EDS samples

SEM-EDS analysis provides detailed insights into the microscopic morphology and chemical composition of the aggregate-asphalt and asphalt-grout ITZ in SFP before and after interface modification. For this purpose, the surface of the SFP sample was sectioned to produce small ITZ specimens, each size approximately 1 cm \times 1 cm \times 0.5 cm. These specimens were embedded in epoxy resin, polished, and cleaned to prepare the final sample for analysis.

3.2. Laboratory experiments

3.2.1. AFM test

A Bruker Dimension ICON machine (Germany) was employed for AFM testing, utilizing a silicon probe. The cantilever had a nominal elastic modulus of 40 N/m, a tip height of $10{-}15~\mu m$, and a tip radius of curvature of 8 nm. The scan area was set to 30 $\mu m \times 30~\mu m$, with a scanning frequency of 0.5 Hz. The Peak Force Quantitative Nanomechanical Mapping (PF-QNM) mode was applied to analyze the AFM results. The DMT modulus, adhesion, and dissipation were used to evaluate the interface properties of the SFP materials.

 Table 3

 Specifications for the laboratory experiment case.

Case	Type	ITZ	Laboratory experiment
1	Original interface	Aggregate-asphalt	AFM, SEM, EDS, NI
2		Asphalt-grout	AFM, SEM, EDS, NI
3	Reinforced interface	Aggregate-asphalt	AFM, SEM, EDS
4		Asphalt-grout	AFM, SEM, EDS, NI

3 2 2 SEM-EDS test

SEM analysis was conducted using accelerated electron scanning at 20 kV on gold-plated samples with a JEM-2100F microscope to examine the microscopic morphology of the aggregate-grout and asphalt-grout ITZ in SFP materials after interface modification. EDS analysis was performed using accelerated electron scanning at 2 kV on non-gold-plated samples with a Tescan LYRA 3 XNU. A line-mode scan was conducted in EDS with a dwell time of 0.1 s to quantitatively characterize the ITZ size in the aggregate-grout and asphalt-grout phases.

3.2.3. NI test

To determine the elastic modulus and evaluate the size of the aggregate-grout and asphalt-grout ITZs in SFP before and after interface modification, a Hysitron Triboindenter TI 980 NI testing machine with a Berkovich tip was used. The maximum load applied was 2 mN, with a loading rate of 0.1 mN/s and a holding time of 2 s. The dwell time was set to 200 s to fully release the creep deformation of the mastic phase during loading. The areas of interest covering aggregate-asphalt ITZ and asphalt-grout ITZ were selected as the indent position of the NI test. Sixteen points were tested for each ITZ, with the layout of these points illustrated in Fig. 5. The light area is the aggregate and asphalt phases, while the dark area is the asphalt phase. The junction area of them can be seen as the ITZ phase. To minimize the effects of residual stress and deformation on subsequent measurements, the interval between each point was set to 40 μm \times 30 μm (column \times interval), ensuring the gradient of the modulus across each ITZ could be accurately captured. The elastic modulus *E* of the ITZs is given by:

$$E = \left(1 - v^2\right) \times \left(\frac{1}{E_r} - \frac{1 - v_i^2}{E_i}\right)^{-1} \tag{1}$$

where E and E_i represent the elastic modulus of the specimen and the indenter, respectively, E_r represents the reduced modulus, while ν and ν_i denote the Poisson's ratio of the specimen and the indenter, respectively.

4. Results

4.1. AFM results

4.1.1. Modulus images

The 3D DMT modulus diagrams of the aggregate-asphalt and asphaltgrout interfaces obtained using AFM, before and after interface immersion, are presented in Fig. 6. In the original aggregate-asphalt interface diagram, a clear boundary between the aggregate and asphalt is observed, indicating minimal material interaction at the microscopic level. The asphalt side exhibits a lower modulus, whereas the aggregate side shows a higher modulus. The modulus values for both sides were statistically analyzed using NanoScope Analysis 1.8 software, and a small area was selected with a modulus value of 3.71 GPa for the asphalt side and 75.84 GPa for the aggregate side. Note the large difference in modulus values between the two sides of the aggregateasphalt interface compared to the asphalt-grout interface. The reason is that the asphalt-grout interface is microscopically violently mixed in the ITZ, with little difference in modulus values between the two sides of the interface. Additionally, some green-speckled areas on the aggregate side suggest minor asphalt infiltration into the aggregate within the aggregate-asphalt ITZ. At the same time, there is little evidence of aggregate infiltration into the asphalt.

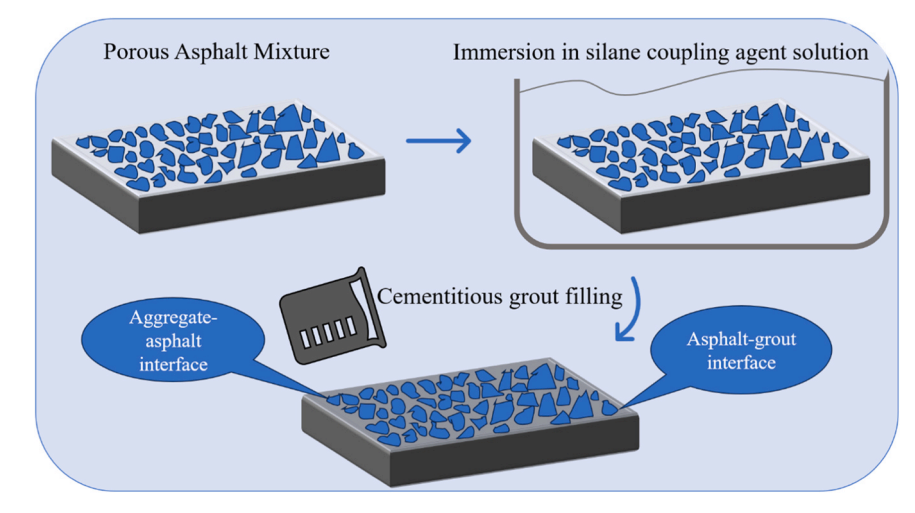


Fig. 2. Flowchart of the interface immersion method using a silane coupling agent.

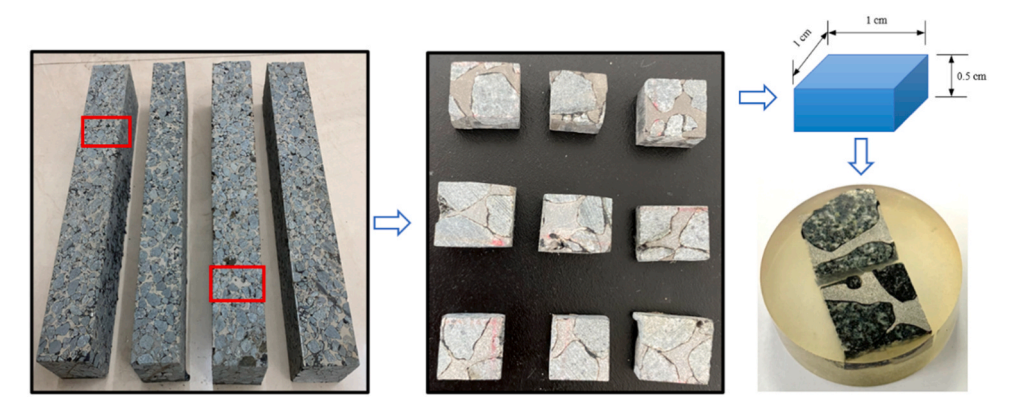


Fig. 3. The pre-processing and the sample of the AFM and NI specimens.

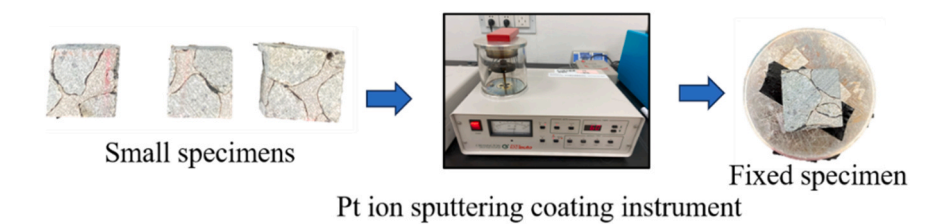


Fig. 4. The preparation of SEM-EDS specimens.

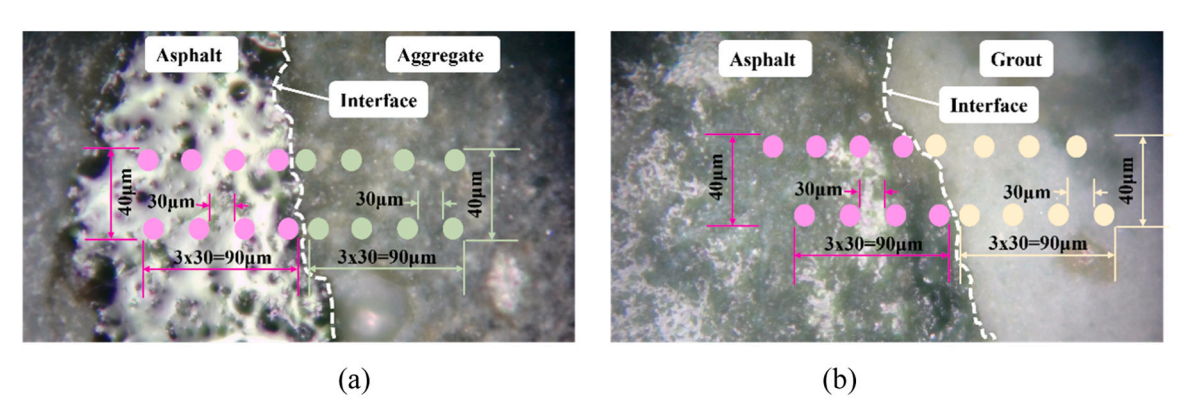
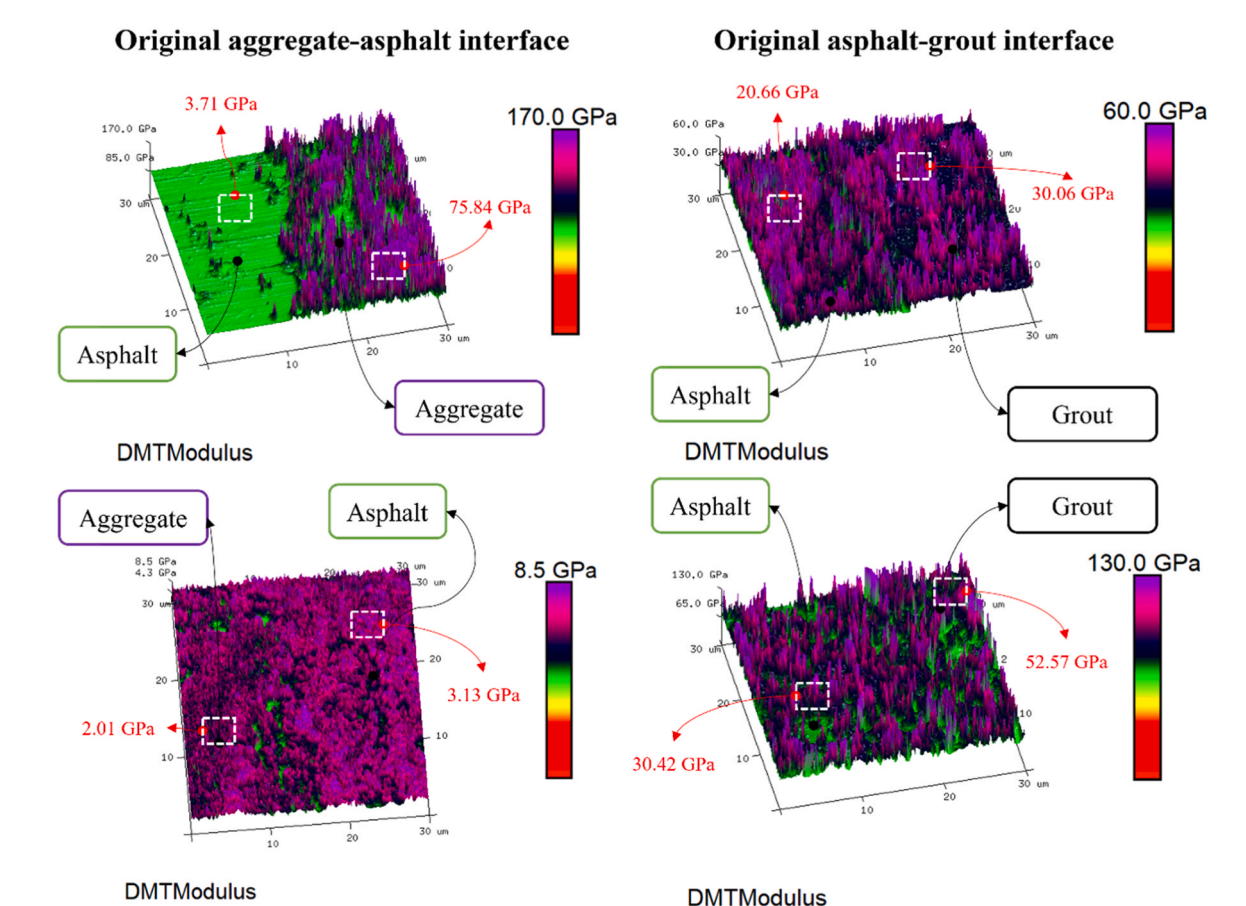


Fig. 5. Illustrate of nanoindentation test: (a) testing area of aggregate-asphalt ITZ, (b) testing area of asphalt-grout ITZ.



Reinforced aggregate-asphalt interface

Reinforced asphalt-grout interface

Fig. 6. 3D map of DMT Modulus distribution in aggregate-asphalt and asphalt-grout ITZs of SFP.

After reinforcement, the aggregate-asphalt interface displays a more uniform modulus distribution with significantly reduced peak values. A faint green low-modulus band appears along the aggregate-asphalt junction, suggesting an enhanced aggregate-asphalt ITZ exceeding 30 μm. This indicates that soaking the porous asphalt mixture specimens in a silane coupling agent solution strengthens the interaction within the transition zone, improving material compatibility and resulting in a more uniform modulus distribution in the ITZ. The same small area was selected and the modulus values were 3.13 GPa on the asphalt side and 2.01 GPa on the aggregate side, at which point there was not much difference in the modulus between the two sides. The asphalt-grout interface also undergoes notable changes after interface immersion. The overall peak modulus within the observed area increases significantly, from 60 GPa to 130 GPa, reflecting intensified material interaction in the ITZ following treatment with the silane coupling agent solution.

4.1.2. Adhesion and dissipation images

Since conventional asphalt pavement materials often suffer from water damage due to reduced adhesion, the adhesion of SFP before and after interface immersion was evaluated in this study. Fig. 7 illustrates the adhesion distribution in the aggregate-asphalt and asphalt-grout ITZs before and after interfacial enhancement. Similarly, a small area was selected for mean statistics. In the original aggregate-asphalt interface, the adhesion on the asphalt side was 120.1 nN and the adhesion on the aggregate side was 30.5nN. In the asphalt-grout interface, the adhesion on the asphalt side was 170.7nN and the adhesion on the grout side was 201.4 nN. In the original ITZs, a distinct boundary is

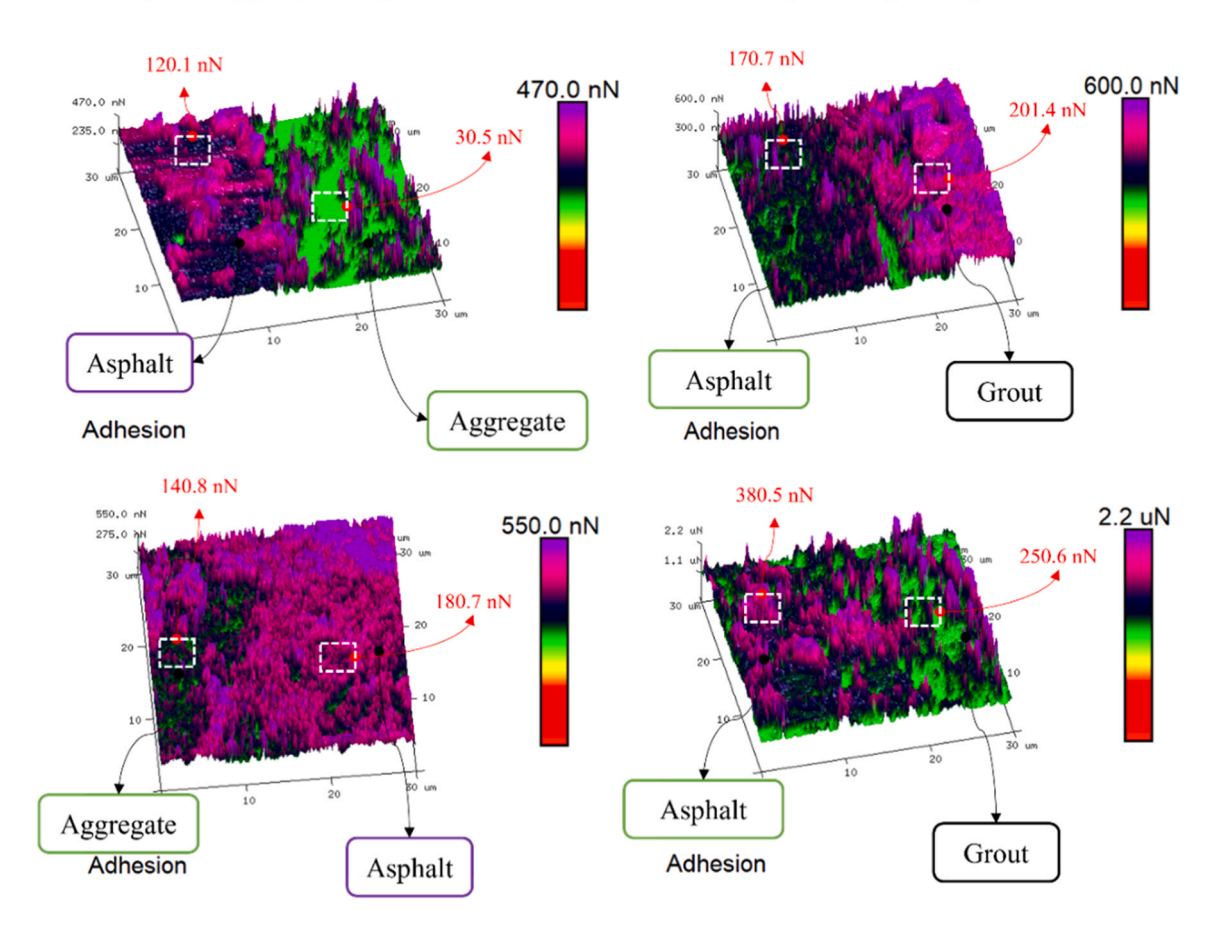
observed. In contrast, the reinforced ITZs exhibit a more staggered and uniform adhesion force distribution, with no clear demarcation and an overall increase in adhesion. After interface enhancement, the adhesion of the aggregate side in the aggregate-asphalt interface is 140.8 nN, and the adhesion of the asphalt side is 180.7nN, while the adhesion of the asphalt side in the asphalt-grout interface is 380.5nN, and the adhesion of the grout side is 250.6 nN, which are significantly increased compared with the original interface, the asphalt-grout interface shows reduced boundary distinction between the asphalt and grout.

The dissipation energy ratio represents the material's stress relaxation capacity, which is crucial for low-temperature performance. Fig. 8 illustrates the dissipation energy maps of both interfaces. The original aggregate-asphalt ITZ maintains a clear boundary, with a dissipation energy of 28.33 keV on the asphalt side and 2.61 keV on the aggregate side, while the asphalt-grout interface has no obvious boundary, and the dissipation energy difference is relatively small. The reinforced aggregate-asphalt interface exhibits no clear boundary, with alternating dispersion of aggregate and asphalt, the dissipation energy on the aggregate side is 20.54 keV, and the dissipation energy on the asphalt side is 32.93 keV, which further confirms the action of the silane coupling agent at the ITZs.

The one-way analysis of variance (ANOVA) is a statistical significance analysis model that examines the significant influence of a factor on experimental results by analyzing single-factor experiment outcomes. Table 4 lists the ANOVA results for the mean values of modulus, adhesion, and dissipation for the AFM test area of the asphalt-aggregate ITZ. All P-values are less than 0.05, indicating that the effect of interface modification on modulus, adhesion, and dissipated energy is statistically

Original aggregate-asphalt interface

Original asphalt-grout interface



Reinforced aggregate-asphalt interface

Reinforced asphalt-grout interface

Fig. 7. Adhesion distribution in aggregate-asphalt and asphalt-grout ITZs of SFP.

significant.

Table 5 shows the ANOVA results before and after modification of the asphalt-grout interface. The ANOVA results confirm that the interface modification significantly enhances the modulus, adhesion force, and dissipated energy of the asphalt-grout ITZ. After modification, the modulus mean increased from 18.95 GPa to 53.14 GPa, the adhesion force mean from 131.00 nN to 295.33 nN, and the dissipation mean from 17.28 keV to 56.17 keV. The p-values for all properties are below 0.01, indicating statistically significant improvements. These findings demonstrate the effectiveness of the silane coupling agent in strengthening the interfacial bonding and improving mechanical performance.

4.2. SEM-EDS results

4.2.1. Microscopic morphology analysis

The SEM images of the aggregate-asphalt and asphalt-grout ITZs phase in SFP are shown in Fig. 9. It reveals prominent microcracks at the asphalt-grout interface, while the aggregate-asphalt interface exhibits strong bonding with a relatively smooth transition. The asphalt-grout interface's microstructure is more complex, featuring a distinct ITZ and two bright bands, indicating more intense microscopic interactions compared to the aggregate-asphalt ITZ, where diffusion is less significant. Additionally, the aggregate at the aggregate-asphalt ITZ appears sharp, rough, and uneven, favoring jagged mechanical interlocking with the asphalt. In contrast, a clear boundary persists at the asphalt-grout ITZ, despite molecular interdiffusion, such as the fly ash diffusion

from grout to asphalt.

Fig. 10 shows the microscopic morphology of the aggregate-asphalt and asphalt-grout ITZs in SFP specimens formed after immersion in the silane coupling agent. Both interfaces exhibit no visible microcracks. The aggregate-asphalt interface contains spherical fly ash, indicating its diffusion into the transition zone, and the aggregate retains its sharp, rough edges, promoting micro-mechanical locking with asphalt. The asphalt-grout ITZ, although gentler in structure, still shows substance diffusion, with composite CA mortar dispersed on the grout side and a bright band at the asphalt edge. Moreover, it can be seen that spherical fly ash and hexagonal calcium hydroxide agglomerates are on the grout side.

4.2.2. Chemical components analysis

Fig. 11 presents the elemental distribution across the aggregate-asphalt ITZ obtained through EDS scanning. A clear boundary is observed at approximately the 75 μm position, where the aggregate, primarily composed of silica (pyroxene), shows higher concentrations of O and Si elements. Metallic elements like Mg, Al, and Fe are also prevalent in the aggregate, but their distribution is interrupted at the 75 μm boundary. Between 75 μm and 130 μm , the elemental distribution becomes discontinuous, with peaks in O, Si, and Mg content indicating the presence of the aggregate-asphalt ITZ. Beyond this zone, other elements show increased peaks, marking the transition to the grout side.

The elemental distribution across the asphalt-grout ITZ using EDS scans of the original SFP specimen is shown in Fig. 12. Distinct elemental

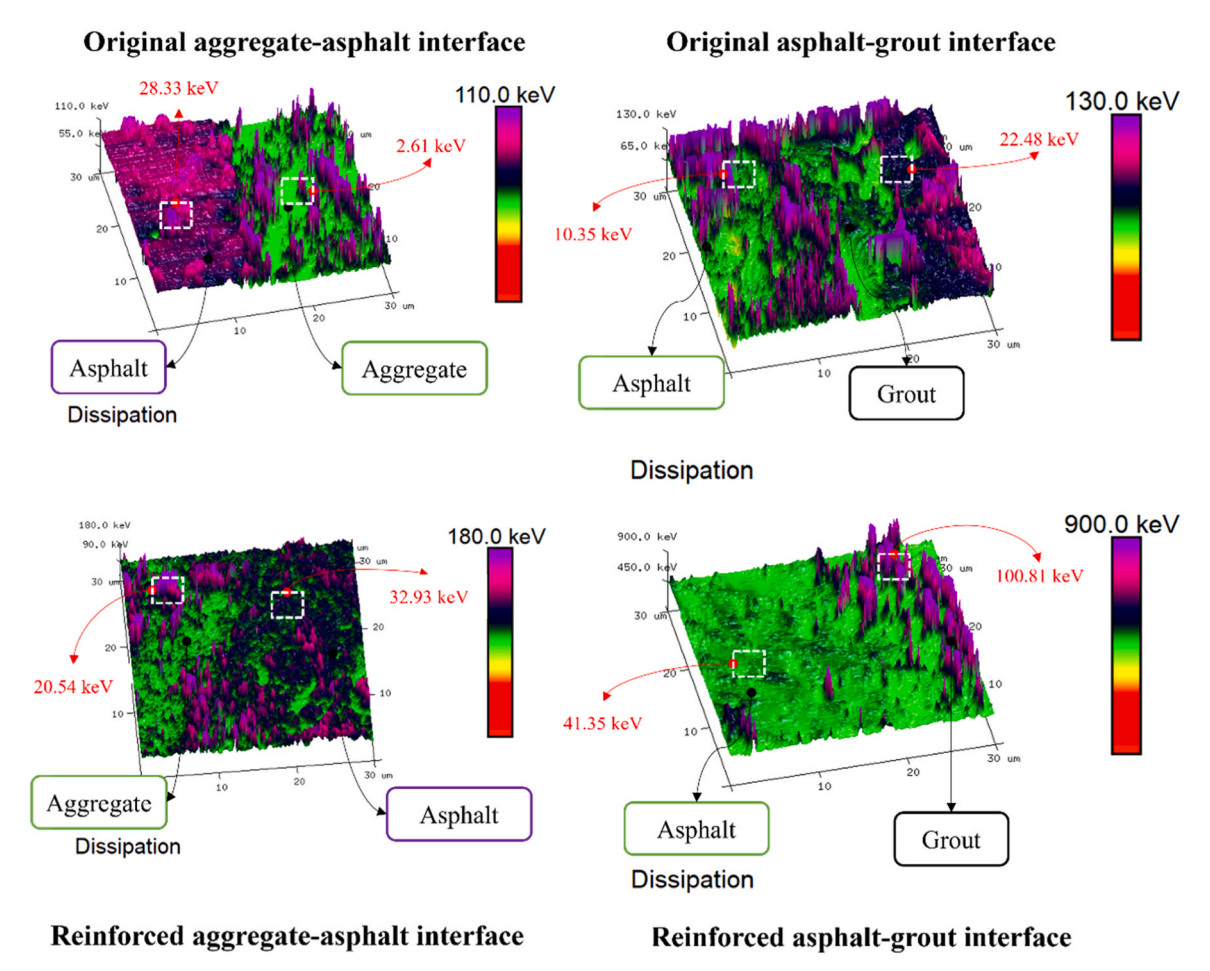


Fig. 8. Dissipation distribution in aggregate-asphalt and asphalt-grout ITZs of SFP.

Table 4
ANOVA results for modulus, adhesion, and dissipated energy in aggregate-asphalt ITZ before and after interface modification.

Parameter	Group	Sample Size (n)	Mean	Variance	F-Value	P-Value	Statistical Significance
Modulus (GPa)	Original interface	3	51.40	67.06	432.96	0.00005	Significant
	Reinforced interface	3	2.49	0.40			
Adhesion (nN)	Original interface	3	292.00	145.33	99.79	0.00056	Significant
	Reinforced interface	3	128.33	625.00			
Dissipation (keV)	Original interface	3	47.60	6.15	122.88	0.00038	Significant
	Reinforced interface	3	21.43	8.66			

Table 5

ANOVA results for the modulus, adhesion force, and dissipated energy in asphalt-grout ITZ before and after interface modification.

Parameter	Group	Sample Size (n)	Mean	Variance	F-Value	P-Value	Statistical Significance
Modulus (GPa)	Original interface	3	18.95	7.76	28.03	0.0061	Significant
	Reinforced interface	3	53.14	117.36			
Adhesion (nN)	Original interface	3	131.00	91.00	322.35	0.00006	Significant
	Reinforced interface	3	295.33	160.33			
Dissipation (keV)	Original interface	3	17.28	8.30	26.82	0.0066	Significant
	Reinforced interface	3	56.17	160.90			

peaks are evident within the ITZ, with Ca aggregating on the grout side and Mg on the asphalt side, along with a significant peak in O content. The elemental distribution within the asphalt remains relatively uniform until decreases in Ca, Si, and W content are noted within the ITZ. In contrast, the grout's elemental distribution is uniform, but significant peaks of Ca, Al, and other elements appear within the ITZ, suggesting the asphalt-grout ITZ spans roughly 65 μ m to 135 μ m. Comparing the two ITZs, the asphalt-grout ITZ demonstrates a denser and more evenly

distributed elemental content than the aggregate-asphalt ITZ. Elemental aggregation patterns differ, with O, Si, and C dominating the aggregate-asphalt ITZ, while Ca, O, and Mg are more prominent in the asphalt-grout ITZ, reflecting the diffusion of elements from the respective materials into their adjacent ITZs.

The elemental distribution at the aggregate-asphalt interface after enhancement of the ITZ in SFP is shown in Fig. 13. The aggregate region is predominantly composed of pyroxene, with high concentrations of O

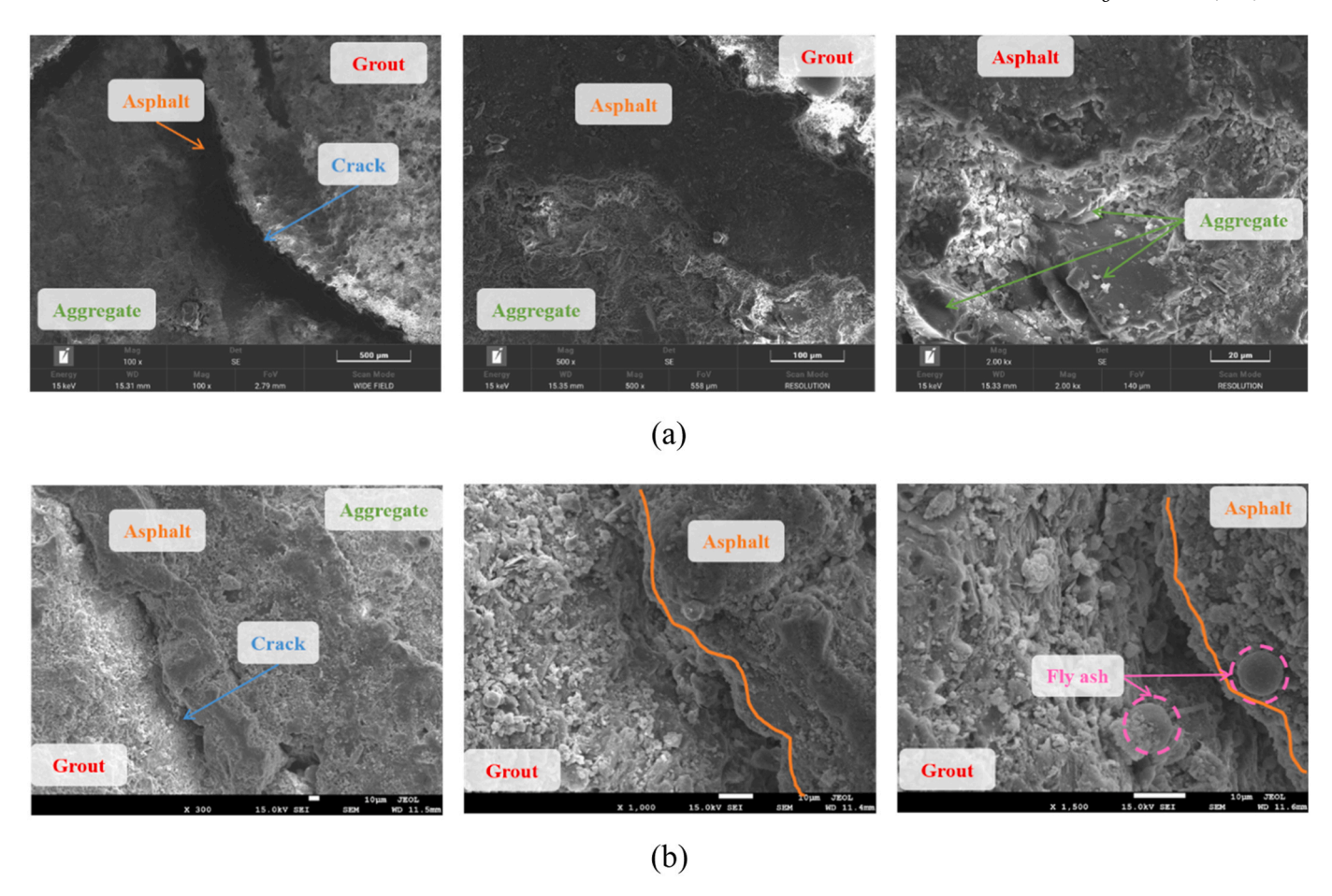


Fig. 9. Microscopic morphology of the original interface between (a) aggregate and asphalt, (b) asphalt and grout materials in SFP.

and Si, along with metal elements such as Mg and Al. At 120 μm , a sharp decline in these elements is noted, while the content of C peaks. From 175 μm , the C content begins to gradually decrease. This suggests that the aggregate-asphalt ITZ spans from 120 μm to 175 μm . Compared to the original ITZ distribution shown in Fig. 11, the enhanced ITZ demonstrates a more uniform and gradual transition, with smoother distributions of C, O, and Si. This indicates that the immersion of the porous asphalt mixture in silane coupling agent solution before grouting has contributed to a more even elemental distribution, integrating the agent into the asphalt and promoting diffusion into the aggregate-asphalt interface. The range of the aggregate-asphalt ITZ remains approximately 60 μm .

Fig. 14 illustrates the elemental distribution at the asphalt-grout interface after enhancing the ITZ in the SFP specimen using EDS scanning. The elemental distribution along the measured line is dense and uniform, with distinct peaks of Si, Al, C, and O in the asphalt-grout ITZ, reflecting the intense elemental diffusion facilitated by the silane coupling agent solution. The enhanced ITZ is estimated to range from 145 μm to 265 μm . Compared to the asphalt-grout ITZ in Fig. 12, the enhanced ITZ shows significant peaks in Si and O, attributed to the silane coupling agent, while Ca and Al tend to accumulate towards the grout. The asphalt-grout ITZ has slightly expanded from the original range of about 80 μm to around 100 μm , with a much denser elemental content, indicating that the silane coupling agent has effectively intensified the elemental distribution, reducing interruptions and broadening the ITZ

The enhancement mechanism of silane coupling agents at the asphalt–cementitious grout interface primarily involves hydrolysis, condensation, chemical bonding, and molecular-level interfacial interactions, as illustrated in Fig. 15. After hydrolysis, silane coupling agents generate silanol groups (Si-OH), which subsequently react with hydroxyl groups (OH $^-$) in the cement hydration phase to form stable Si–O–Si or Si–O–Ca bonds. This chemical reaction strengthens the adhesion between the silane-modified interface and the cementitious matrix, reinforcing the microstructural integrity of the grout. Meanwhile, the organic functional groups of silane molecules interact with the polar components of asphalt through hydrogen bonding, Van der Waals forces, or covalent interactions, thereby enhancing interfacial compatibility. This dual interaction mechanism not only improves interfacial bonding but also reduces porosity, mitigates moisture-induced degradation, and enhances shear resistance and fatigue performance. Consequently, the incorporation of silane coupling agents leads to a more durable and resilient semi-flexible pavement structure by optimizing interfacial adhesion and minimizing water-induced damage.

4.3. NI results

The contour map of the elastic modulus in the ITZs of SFP specimens before and after interface modification are shown in Fig. 16. The AFM and SEM-EDS analyses in Sections 4.1 and 4.2 indicate minimal changes in the modulus and dimensions of the aggregate-asphalt ITZ before and after interface modification. Thus, only the original results of the aggregate-asphalt ITZ are presented in Fig. 15. The red areas denote regions with higher elastic modulus, whereas the blue areas represent regions with lower elastic modulus. Although only a few points were initially tested, Fig. 16 reveals that the elastic modulus distribution in the aggregate and grout is irregular, while the distribution in the three ITZ types, i.e., original aggregate-asphalt ITZ, original asphalt-grout ITZ, and reinforced asphalt-grout ITZ, appears more regular.

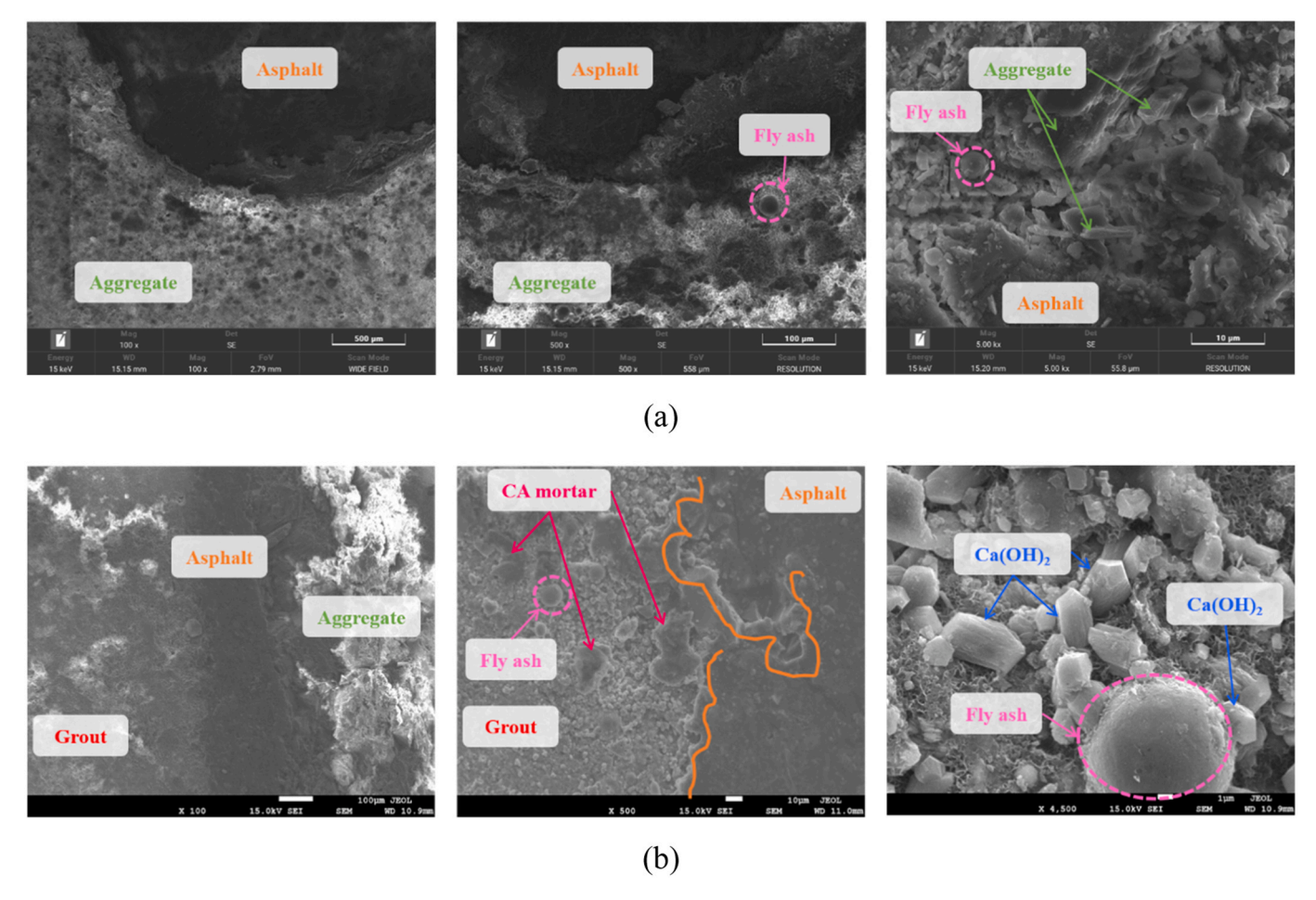


Fig. 10. Microscopic morphology of the reinforced interface between (a) aggregate and asphalt, (b) asphalt and grout materials in SFP.

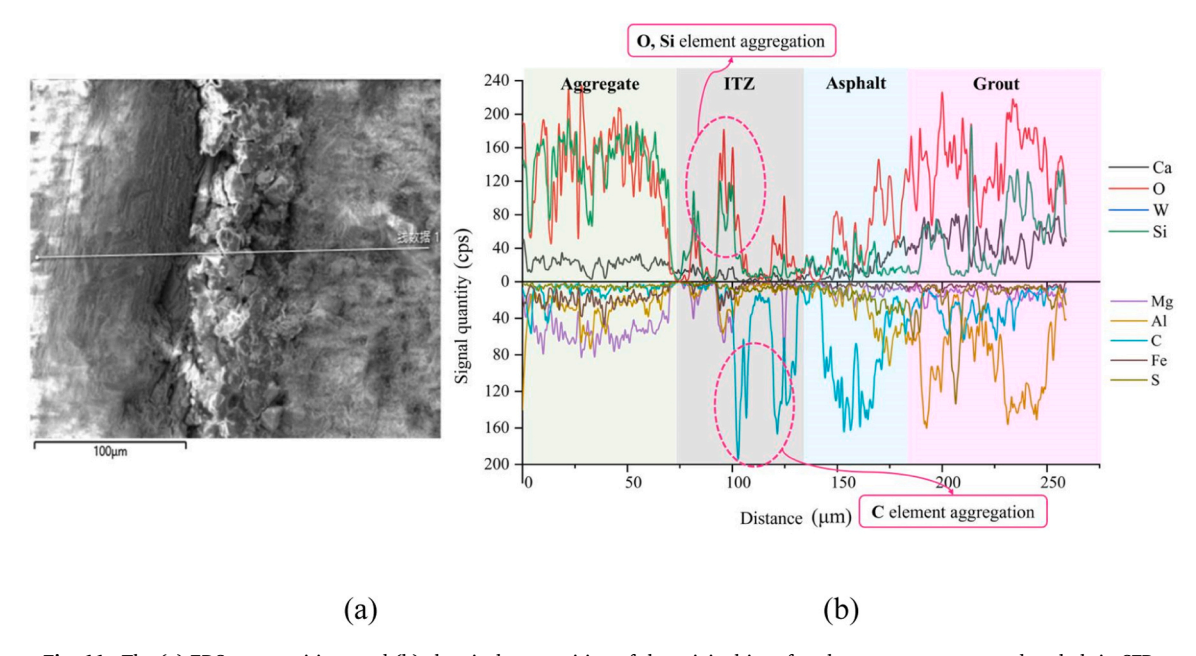


Fig. 11. The (a) EDS scan positions and (b) chemical composition of the original interface between aggregate and asphalt in SFP.

Fig. 17 illustrates the widths of the ITZs: the aggregate-asphalt ITZ measures about 60–90 μm , the original asphalt-grout ITZ is approximately 60–90 μm , and the reinforced asphalt-grout ITZ spans 90–120 μm . The results indicate that the modulus in the reinforced asphalt-grout

ITZ is higher than in the aggregate-asphalt ITZ, and the width of the reinforced asphalt-grout ITZ is greater than that of the original asphalt-grout ITZ after interface modification. These findings are consistent with the SEM-EDS results. In conclusion, the grout materials exert a stiffening

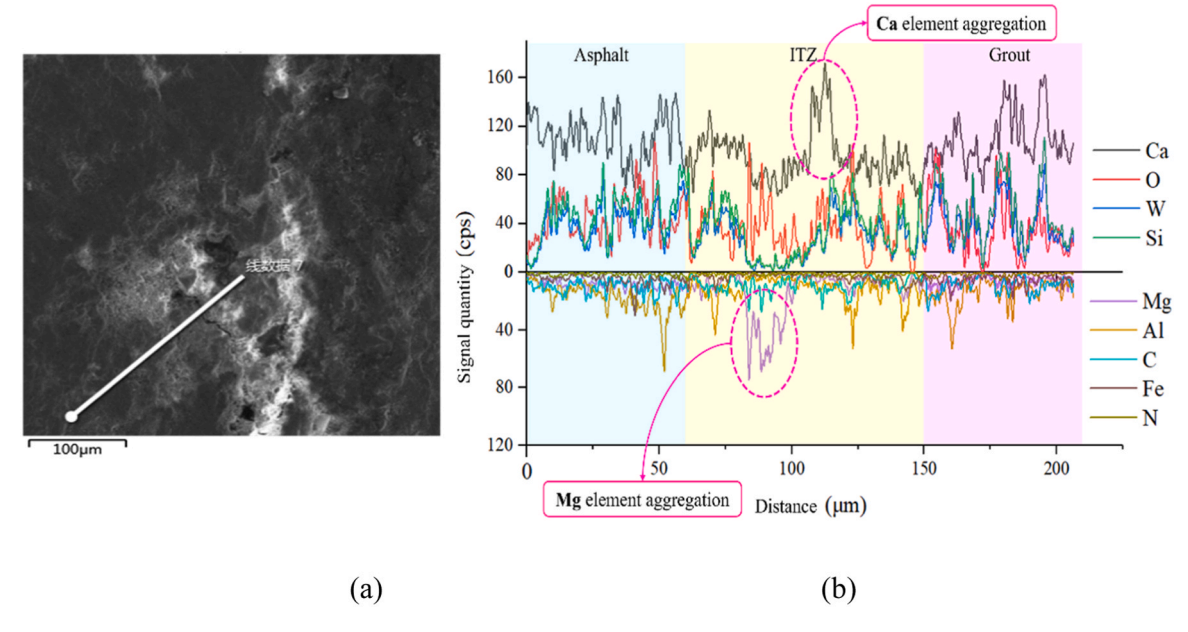


Fig. 12. The (a) EDS scan positions and (b) chemical composition of the original interface between asphalt and grout in SFP.

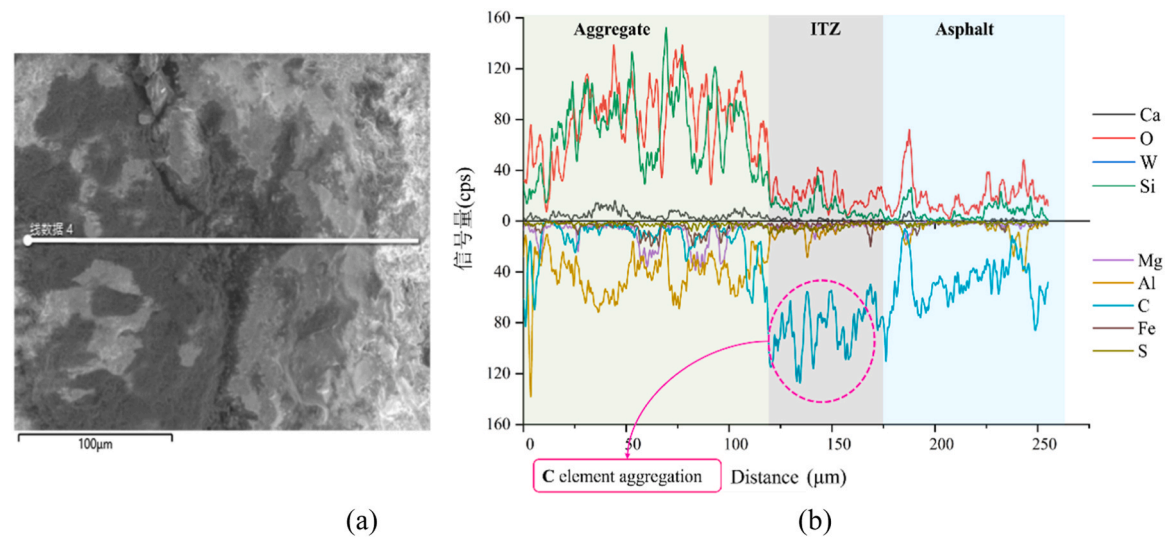


Fig. 13. The (a) EDS scan positions and (b) chemical composition of the reinforced interface between aggregate and asphalt in SFP.

effect on the asphalt-grout ITZ, with the modulus of the asphalt-grout phase being approximately double that of the aggregate-asphalt phase. Interface modification using a silane coupling agent increases both the modulus and the width of the reinforced asphalt-grout ITZ compared to the original asphalt-grout ITZ.

4.4. Comparative study

Table 6 summarizes the results of the four tests conducted in this study, showing consistent trends across five indicators, *i.e.*, adhesion, dissipation, interface modulus, number of microcracks, and interface width, before and after interface enhancement. The findings indicate minimal changes in the microscopic properties of the aggregate-asphalt ITZ following interface enhancement. However, the asphalt-grout ITZ shows significant improvements, with increased modulus, adhesion, and ITZ width, enhancing interface interactions and overall interface strength. The SEM tests demonstrate a visible reduction in microcracks within the asphalt-grout ITZ after interface modification. Concordant

conclusions were drawn from AFM and NI tests regarding the interface modulus and adhesion properties of the SFP. Similarly, EDS and NI tests yielded consistent results about the ITZ width of the SFP composite interface. This analysis suggests that these four testing methods can systematically and accurately assess the microscopic properties of the composite interface in SFP materials.

Fig. 18 presents a combined analysis of the changes in the two interfaces in the SFP before and after grout molding using silane coupling agent solution immersion. The aggregate-asphalt ITZ dimensions remain largely unchanged, while the asphalt-grout ITZ dimensions grow and widen, with calcium hydroxide and fly ash in the asphalt-grout ITZ diffusing further into the asphalt and even into the aggregate-asphalt ITZ. This enhancement in the chemical bonding between components is attributed to the silane coupling agent solution, which improves material dispersion and integration, particularly in the asphalt-grout ITZ.

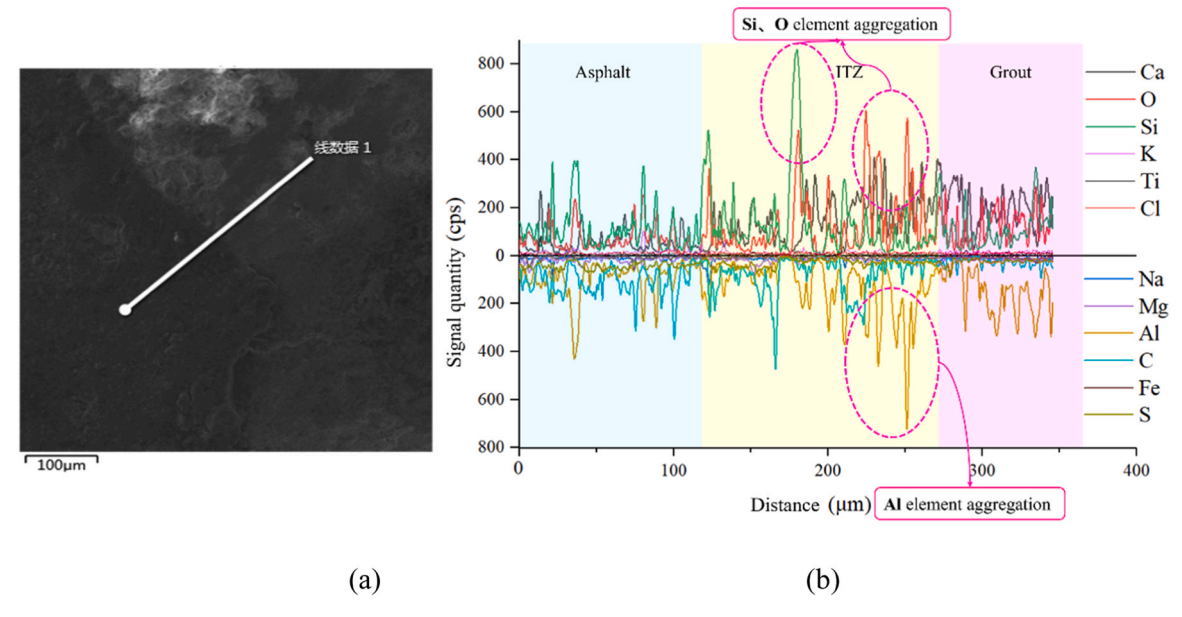


Fig. 14. The (a) EDS scan positions and (b) chemical composition of the reinforced interface between asphalt and grout in SFP.

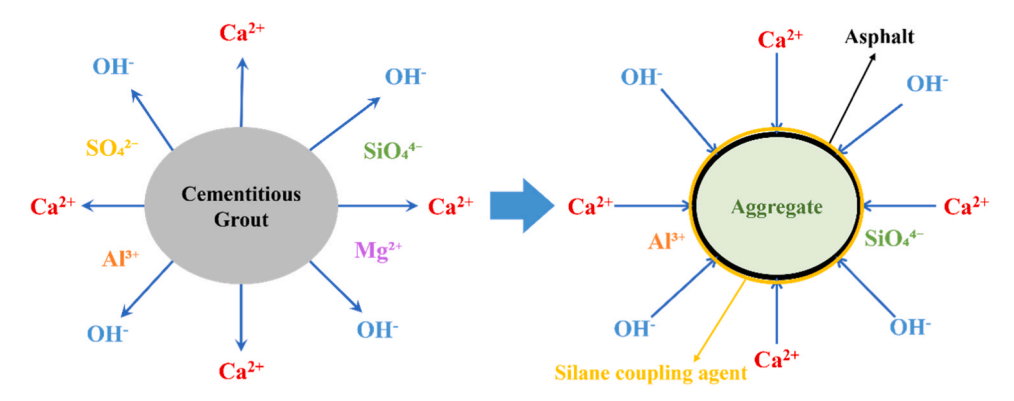


Fig. 15. Hydration reaction of cement grout materials and chemical action mechanism of silane coupling agent.

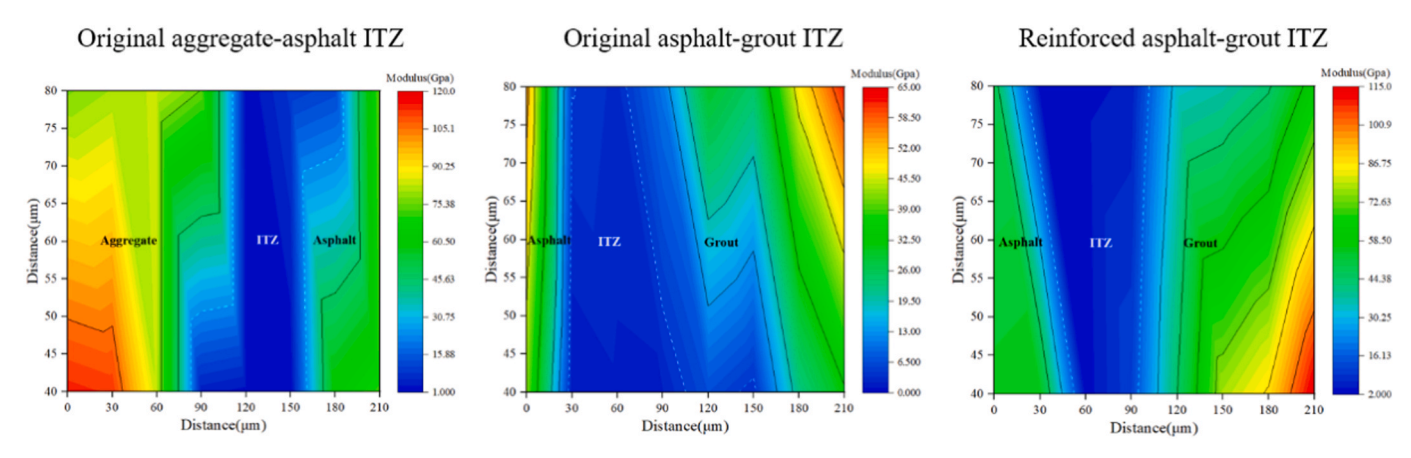


Fig. 16. The contour map of elastic modulus in aggregate-asphalt and asphalt-grout ITZs of SFP.

5. Conclusions

This paper investigates the micro- and nano-scale performance of composite interfaces in SFP material. To enhance the mechanical properties of the ITZ, an immersion method involving the use of a silane coupling agent with PAM is proposed. The aggregate-asphalt and

asphalt-grout ITZs in SFP material are analyzed through various tests, including AFM for adhesion performance, SEM for microscopic morphology, EDS for chemical composition, and NI for interface characterization. The key conclusions from the analyses are as follows:

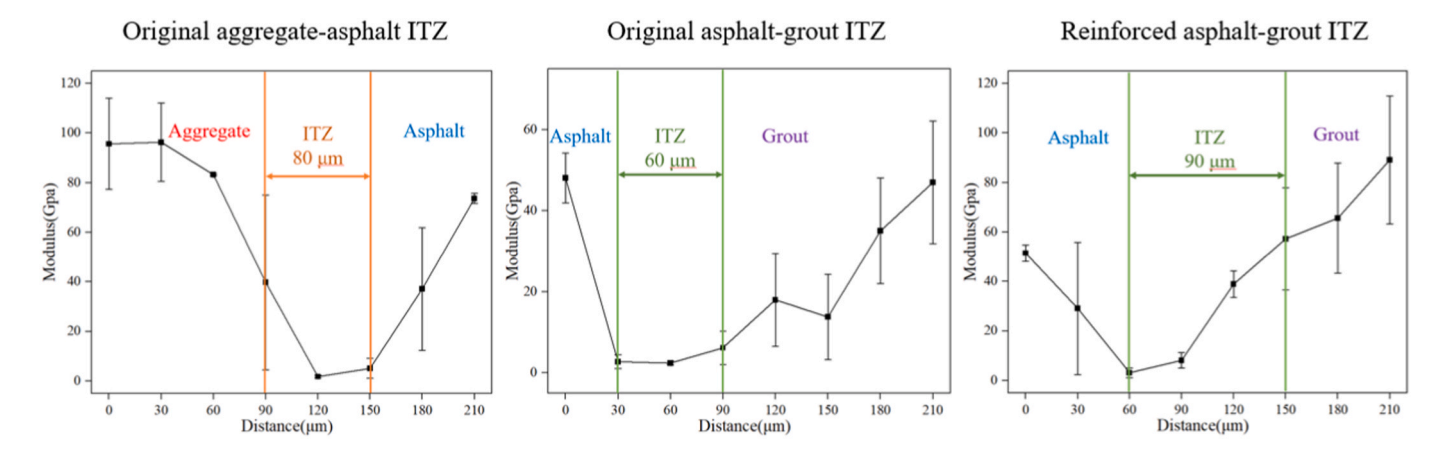


Fig. 17. Elastic modulus in aggregate-asphalt and asphalt-grout ITZs of SFP.

Table 6Comparison of index ratio of different ITZ in SFP materials.

Test	Index ratio	Original interface vs Reinforced interface		
		aggregate-asphalt ITZ	Asphalt-grout ITZ	
AFM	Modulus	<	<	
	Adhesion	≈	<	
	Dissipation	≈	<	
SEM	Micro cracks	≈	<	
EDS	ITZ width	≈	<	
NI	ITZ width	/	<	
	Modulus	/	<	

- (1) The aggregate-asphalt ITZ shows minimal interaction before and after interface enhancement. The primary interaction in the SFP composite interface occurs within the asphalt-grout ITZ, which exhibits superior adhesion compared to the aggregate-asphalt ITZ.
- (2) Grout diffusion in the asphalt-grout ITZ is more pronounced than in the aggregate-asphalt ITZ, both before and after interface reinforcement. Cracks are more prevalent in the asphalt-grout ITZ; however, they are significantly reduced following interface reinforcement.
- (3) The element distribution in the aggregate-asphalt ITZ is relatively uniform, with a gradual transition, while the asphalt-grout ITZ shows a denser element distribution. The proposed surface immersion method promotes a more continuous element

- distribution in the asphalt-grout ITZ, thereby enhancing the mechanical properties of the SFP composite interface.
- (4) The width of the aggregate-asphalt ITZ remains relatively constant before and after modification (approximately 60–90 μm), whereas the asphalt-grout ITZ experiences a significant increase in width after interface modification (from 60 to 90 μm to 90–120 μm).
- (5) The enhancement of the asphalt-grout ITZ is driven by hydrolysis, condensation, and chemical bonding of silane coupling agents, which strengthen adhesion and microstructural integrity. This dual interaction mechanism, involving chemical bonding with the cementitious matrix and molecular interactions with asphalt, improves compatibility, reduces porosity, and enhances ITZ strength.

CRediT authorship contribution statement

Liu Xiaoyu: Writing – original draft, Software, Methodology, Data curation. Ni Botao: Funding acquisition, Formal analysis. Wu Kuanghuai: Supervision, Resources. Ren Fengming: Writing – review & editing, Resources, Funding acquisition, Formal analysis. Li Yi: Writing – review & editing, Supervision. Cai Xu: Writing – review & editing, Resources, Conceptualization. Yue Yunpeng: Writing – review & editing, Investigation, Conceptualization.

Declaration of Competing Interest

The authors declare that they have no known competing financial

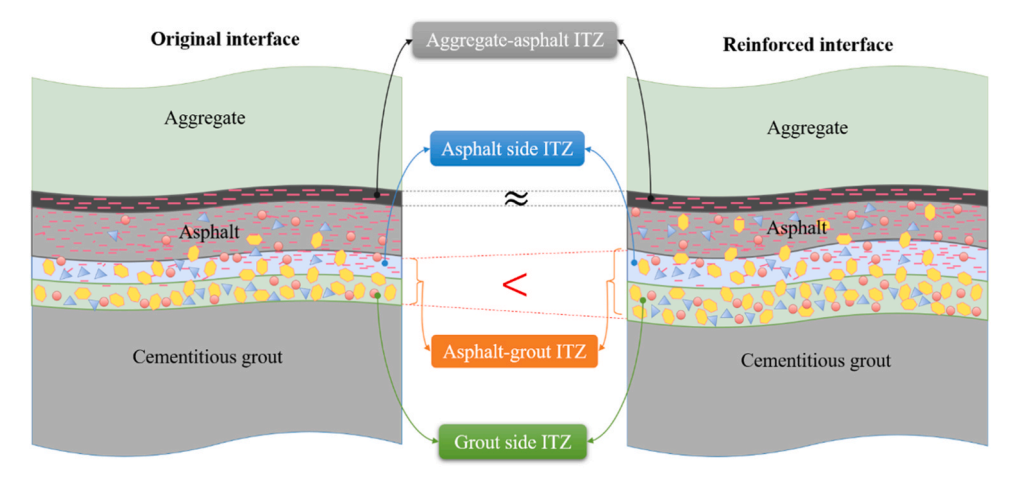


Fig. 18. Illustration of the aggregate-asphalt and asphalt-grout ITZs in the microstructure of SFP materials before and after interface modification.

interests or personal relationships that could have appeared to influence the work reported in this paper.

Acknowledgments

The work described in this paper is supported by the National Natural Science Foundation of China (No. 52338005, 51878193). China Postdoctoral Science Foundation (No. 2024M760619).

Data availability

Data will be made available on request.

References

- M.M. Disfani, A. Mohammadinia, G.A. Narsilio, L. Aye, Performance evaluation of semi-flexible permeable pavements under cyclic loads, Int. J. Pavement Eng. 21 (2020) 336–346.
- [2] Z. Zhao, L. Xu, X. Li, X. Guan, F. Xiao, Comparative analysis of pavement performance characteristics of flexible, semi-flexible and rigid pavement based on accelerated pavement tester, Constr. Build. Mater. 387 (2023) 131672.
- [3] A. Hassani, M. Taghipoor, M.M. Karimi, A state of the art of semi-flexible pavements: Introduction, design, and performance, Constr. Build. Mater. 253 (2020) 119196.
- [4] J. Song, B. Chen, M. Sun, K. Wu, J. Chen, X. Cai, Study on the improvement of fatigue and crack resistance of semi-flexible pavement materials using the mixingmolding method, Constr. Build. Mater. 450 (2024) 138728.
- [5] I. Abdulsahib, M.M. Hilal, M.Y. Fattah, Semi-flexible pavement: a review of design and performance evaluation, E3S Web Conf., EDP Sci. (2023) 03001.
- [6] R.I. Al-Nawasir, B.H. Al-Humeidawi, A scientometric study and a bibliometric review of the literature on the design and construction of semi-flexible pavement, Al-Qadisiyah J. Eng. Sci. 16 (2023) 30772, 10.
- [7] Z. Chen, S. Ling, D. Sun, L. Xu, Y. Wu, Research on cracking characteristics and failure modes of semi-flexible pavement materials, Constr. Build. Mater. 452 (2024) 138915.
- [8] W. Zhao, Q. Yang, Influence analysis of performance of semi-flexible pavement based on aggregate distribution characteristics of matrix skeleton, Constr. Build. Mater. 338 (2022).
- [9] D. Jiang, D. Wang, Z. Chen, L. Fan, J. Yi, Research on the mesoscopic viscoelastic property of semi-flexible pavement mixture based on discrete element simulation, Case Stud. Constr. Mater. 17 (2022).
- [10] X. Liu, K. Wu, G. Giacomello, X. Cai, M. Pasetto, Numerical analysis of mechanical properties at the internal interface of SFP material using a digital image algorithm, Mater. Struct. 58 (2025).
- [11] M.S. Raza, S.K. Sharma, A review of mechanical and durability properties and microstructure of semi-flexible pavement, Innov. Infrastruct. Solut. 9 (2024).
- [12] X. Guo, P. Hao, Influential factors and evaluation methods of the performance of grouted semi-flexible pavement (GSP)—a review, Appl. Sci. 11 (2021) 6700.
- [13] J. Xu, C. Kong, T. Xu, Displacemental and mesomechanical responses of semi-flexible pavement based on discrete element method, Int. J. Pavement Res. Technol. (2021) 1–14.
- [14] C. Songqiang, Z. Jian, W. Xi, C. Zining, Research on innovative preparation and performance of semi flexible pavement materials, Case Stud. Constr. Mater. 20 (2024)
- [15] L. Zhang, S. Zhou, Z. Xiong, Z. Mo, Q. Lu, J. Hong, Research on the crack resistance of semi-flexible pavement mixture based on meso-heterogeneous model, Constr. Build. Mater. 411 (2024).

- [16] M. Zhang, Z. Xiong, M. Gong, J. Hong, H. Qiao, Y. Zhang, L. jiang, Multi-scale damage characterisation of semi-flexible pavements under freeze-thaw cycles, Constr. Build. Mater. 445 (2024).
- [17] K. Wu, X. Liu, X. Cai, W. Huang, J. Yu, G. Nie, Performance and fracture analysis of composite interfaces for semi-flexible pavement, Coatings 11 (2021).
- [18] X. Cai, Z. Leng, P.K. Ashish, C. Shi, J. Yang, M. Gong, Temperature dependency analysis of the fracture characteristics of semi-flexible pavement (SFP) mixtures using acoustic emission technique, Int. J. Pavement Eng. 24 (2023) 2201903.
- [19] M. Gong, Z. Xiong, H. Chen, C. Deng, X. Chen, J. Yang, H. Zhu, J. Hong, Evaluation on the cracking resistance of semi-flexible pavement mixture by laboratory research and field validation, Constr. Build. Mater. 207 (2019) 387–395.
- [20] X. Cai, L. Fu, J. Zhang, X. Chen, J. Yang, Damage analysis of semi-flexible pavement material under axial compression test based on acoustic emission technique, Constr. Build. Mater. 239 (2020).
- [21] R. Al-Nawasir, B. Al-Humeidawi, A. Shubbar, Influence of sustainable grout material on the moisture damage of semi-flexible pavement, Period. Polytech. Civ. Eng. (2024).
- [22] Y. Yang, S.L. Huang, Q.J. Ding, X.Y. Peng, The property research on interfacial modificated semi-flexible pavement material, Appl. Mech. Mater. 71-78 (2011) 1090–1098
- [23] B. Chen, H. Shao, B. Li, Z. Li, Influence of silane on hydration characteristics and mechanical properties of cement paste, Cem. Concr. Compos. 113 (2020) 103743.
- [24] X. Liu, K. Wu, X. Cai, W. Huang, J. Huang, Influence of the composite interface on the mechanical properties of semi-flexible pavement materials, Constr. Build. Mater. 397 (2023).
- [25] X. Liu, K. Wu, G. Giacomello, Y. Yue, F. Ren, X. Cai, M. Pasetto, Enhancing cracking resistance in semi-flexible pavements using an interfacial immersion method, Case Stud. Constr. Mater. (2025) e04311.
- [26] L. Loeber, O. Sutton, J. Morel, J.M. Valleton, G. Muller, New direct observations of asphalts and asphalt binders by scanning electron microscopy and atomic force microscopy, J. Microsc. 182 (1996) 32–39.
- [27] M. Mazumder, R. Ahmed, A.W. Ali, S.-J. Lee, SEM and ESEM techniques used for analysis of asphalt binder and mixture: a state of the art review, Constr. Build. Mater. 186 (2018) 313–329.
- [28] X. Chang, S. Liu, C. Zhang, P. Shen, D. Xuan, X. Guan, C. Shi, Carbonation-hardening properties and ITZ microstructure of low-calcium CO2 sequestration binder mortar, Constr. Build. Mater. 336 (2022).
- [29] F. Karim, J. Hussain, I. Hafeez, Estimating the Asphalt Binder Film Thickness Using Scanning Electron Microscope and Energy Dispersive X-Ray Spectroscopy, Adv. Mater. Sci. Eng. 2021 (2021) 8894970.
- [30] Y. Veytskin, C. Bobko, C. Castorena, Y.R. Kim, Nanoindentation investigation of asphalt binder and mastic cohesion, Constr. Build. Mater. 100 (2015) 163–171.
- [31] Z. Du, X. Zhu, Y. Yuan, Molecular investigation on the adhesion and deformation behaviors of asphalt binder under nanoindentation, Constr. Build. Mater. 295 (2021) 123683.
- [32] Z. Yao, G. Lu, J. Yang, M. Gong, Z. Tang, J. Xue, X. Zhang, Nanoindentation characterization of aging gradient of mastic in asphalt mixtures, Constr. Build. Mater. 214 (2019) 187–195.
- [33] X. Lv, W. Fan, J. Wang, M. Liang, C. Qian, H. Luo, G. Nan, B. Yao, P. Zhao, Study on adhesion of asphalt using AFM tip modified with mineral particles, Constr. Build. Mater. 207 (2019) 422–430.
- [34] Q. Huang, Z. Qian, J. Hu, D. Zheng, L. Chen, M. Zhang, J. Yu, Investigation on the properties of aggregate-mastic interfacial transition zones (ITZs) in asphalt mixture containing recycled concrete aggregate, Constr. Build. Mater. 269 (2021).
- [35] M.o.T.o.t.P.s.R.o. China, Standard Test Methods of Bitumen and Bituminous Mixtures for Highway Engineering, China, 2011.
- [36] M.o.T.o.t.P.s.R.o. China, Test methods of cement and concrete for highway engineering, Industry Standard, China, 2020.